THE FASEB JOURNAL • RESEARCH • www.fasebj.org

Mechanoregulation of p38 activity enhances endoplasmic reticulum stress–mediated inflammation by arterial endothelium

Keith A. Bailey,* Emily Moreno,* Fawaz G. Haj,†,‡ Scott I. Simon,* and Anthony G. Passerini*,[1]

*Department of Biomedical Engineering, †Department of Nutrition, and ‡Department of Internal Medicine, University of California–Davis, Davis, California, USA

ABSTRACT: Endothelial up-regulation of VCAM-1 at susceptible sites in arteries modulates the recruitment efficiency of inflammatory monocytes that initiates atherosclerotic lesion formation. We reported that hydrodynamic shear stress (SS) mechanoregulates inflammation in human aortic endothelial cells through endoplasmic reticulum (ER) stress *via* activation of the transcription factor x-box binding protein 1 (XBP1). Here, a microfluidic flow channel that produces a linear gradient of SS along a continuous monolayer of endothelium was used to delve the mechanisms underlying transcriptional regulation of TNF-α–stimulated VCAM-1 expression. High-resolution immunofluorescence imaging enabled continuous detection of platelet endothelial cell adhesion molecule 1 (PECAM-1)–dependent, outside-in signaling as a function of SS magnitude. Differential expression of VCAM-1 and intercellular adhesion molecule 1 (ICAM-1) was regulated by the spatiotemporal activation of MAPKs, ER stress markers, and transcription factors, which was dependent on the mechanosensing of SS through PECAM-1 and PI3K. Inhibition of p38 specifically abrogated the rise to peak VCAM-1 at low SS (2 dyn/cm^2), whereas inhibition of ERK1/2 attenuated peak ICAM-1 at high SS (12 dyn/cm^2). A shear stress–regulated temporal rise in p38 phosphorylation activated the nuclear translocation of XBP1, which together with the transcription factor IFN regulatory factor 1, promoted maximum VCAM-1 expression. These data reveal a mechanism by which SS sensitizes the endothelium to a cytokine-induced ER stress response to spatially regulate inflammation promoting atherosclerosis.—Bailey, K. A., Moreno, E., Haj, F. G., Simon, S. I., Passerini, A. G. Mechanoregulation of p38 activity enhances endoplasmic reticulum stress–mediated inflammation by arterial endothelium. FASEB J. 33, 12888–12899 (2019). www.fasebj.org

KEY WORDS: mechanotransduction · shear stress · VCAM-1 · MAPK · atherosclerosis

Atherosclerotic cardiovascular disease is the leading cause of death and disability globally (1). Atherosclerosis manifests as a focal inflammation of the artery wall that spatially correlates with sites exposed to disturbed blood flow, notably low magnitude, and oscillatory wall shear stress (SS). Among the earliest changes that functionally promote lesion formation at these susceptible sites is endothelial cell (EC) membrane up-regulation of VCAM-1, which serves as a counter-receptor for very late antigen-4–dependent monocyte recruitment from the circulation. Mouse models of atherosclerosis and human postmortem studies confirm that ECs at atherosusceptible sites corresponding to low SS express high levels of VCAM-1 and capture monocytes more efficiently compared with arterial regions that experience unidirectional flow and high SS (2–6). Likewise, differential regulation of VCAM-1 transcription and expression is exhibited by TNF-α–activated human aortic ECs (HAECs) exposed to high *vs.* low or flow-reversing SS, and this directly influences the extent of inflammatory monocyte recruitment *ex vivo* (7–9). In contrast, intercellular adhesion molecule 1 (ICAM-1) expression, enhanced by high SS, promotes lymphocyte function–associated antigen 1–mediated neutrophil recruitment and plays a less prominent role in atherogenesis. Key to understanding atherogenic susceptibility at focal regions in arteries is revealing how the shear forces of blood flow sensed at the cell membrane are transduced into biochemical signals that precisely regulate the endothelial inflammatory phenotype.

The endoplasmic reticulum (ER) functions in the processing, packaging, and transportation of lipids and

ABBREVIATIONS: CAM, cell adhesion molecule; EC, endothelial cell; eIF2α, eukaryotic initiation factor 2α; ER, endoplasmic reticulum; HAEC, human aortic EC; ICAM-1, intercellular adhesion molecule 1; IRF-1, IFN regulatory factor 1; MKP-1, MAPK phosphatase 1; PECAM-1, platelet EC adhesion molecule 1; shRNA, short hairpin RNA; SS, shear stress; UPR, unfolded protein response; XBP1, x-box binding protein 1; XBP1s, spliced XBP1

[1] Correspondence: Department of Biomedical Engineering, University of California–Davis, 451 Health Sciences Dr., GBSF 3319, Davis, CA 95616, USA. E-mail: agpasserini@ucdavis.edu

doi: 10.1096/fj.201900236R

0892-6638/19/0033-12888 © FASEB

proteins within the cell. Metabolic overload induces a state of ER stress and downstream responses that link dysregulated metabolism with endothelial dysfunction and inflammation promoting atherosclerosis (7, 10–12). The ER stress response constitutes a set of conserved signaling pathways to maintain proteostasis, termed the unfolded protein response (UPR). The signaling that characterizes the UPR includes activation of inositol-requiring enzyme 1α, leading to the splicing of x-box binding protein 1 (XBP1) to produce the active form of this transcription factor [spliced XBP1 (XBP1s)], and phosphorylation of protein kinase-like ERK, which subsequently leads to activation of eukaryotic initiation factor 2α (eIF2α) (13). Canonically, the UPR signals a range of responses to alleviate ER stress and restore equilibrium.

Studies in swine and apolipoprotein E–null mice fed a high-fat diet have revealed a chronic state of ER stress and activation of the UPR at atherosusceptible sites and within atherosclerotic lesions (10, 13). A study in cultured ECs confirmed a role for atherosusceptible-fluid SS in modulating an ER stress response (11). Although the mechanisms that link mechanotransduction of SS with the ER-mediated inflammatory responses that promote atherosclerosis are unknown, we have established that low-magnitude SS is a potent inducer of the ER stress response in TNF-α–inflamed HAEC that is dependent on the transmembrane glycoprotein platelet endothelial cell adhesion molecule 1 (PECAM-1) (7). Specifically, low SS signals through the UPR transcription factors XBP1 and eIF2α to potentiate the TNF-α response by eliciting maximal IFN regulatory factor 1 (IRF-1)–dependent VCAM-1 expression and monocyte adhesion to HAEC (7). In contrast, the expression of ICAM-1 by high SS is independent of both IRF-1 and ER stress (7, 14). These findings motivated the current study to elucidate how the magnitude of SS sensed by PECAM-1 is mechanotransduced to modulate the ER stress response in regulating the level of VCAM-1 expression, which is distinct from a mechanism that influences spatial regulation of ICAM-1 expression.

Mechanotransduction in ECs involves adhesion receptors that are integral to the sensing of the magnitude of hemodynamic stress and converting it into biochemical signals that regulate cellular responses. These receptors include PECAM-1 at cell junctions and integrins that anchor ECs to the extracellular matrix. PECAM-1 is established as a force transducer that complexes with the adaptor protein vascular endothelial cadherin to trigger activation of the Src family kinase that phosphorylates and activates VEGF receptor 2, independent of receptor ligation (15, 16). Activated VEGF receptor 2 signals *via* PI3K to activate downstream pathways including the conversion of integrins to a high-affinity state. Integrin activation, in turn, signals *via* multiple pathways to regulate EC function (15–17). Inhibition of PECAM-1 expression was shown to abrogate the SS-dependent regulation of both VCAM-1 and ICAM-1 expression in TNF-α–inflamed HAECs (7). Elusive are the downstream pathways that regulate the differential expression patterns of these adhesion receptors on arterial ECs as a function of the magnitude of SS. This is directly relevant to elucidating the mechanobiology of plaque formation at hemodynamically susceptible regions in arteries.

MAPKs are a set of evolutionarily conserved serine-threonine kinases including p38, JNK, and ERK1/2, which signal extracellular stimuli to control a host of cellular responses, including the activation of transcription factors. MAPK activation is tightly controlled by kinase phosphorylation and phosphatase dephosphorylation, and the dynamics of this process are known to influence transcription of inflammatory mediators (18). The MAPKs p38 and ERK1/2 are transiently phosphorylated in response to high-magnitude SS, beginning 2 min after the onset of flow, peaking at 5–15 min, and returning to baseline (19–22). The SS regulation of MAPKs has been linked to modulation of EC functions including prostaglandin I_2 secretion, cell alignment, and cell adhesion molecule (CAM) expression (17, 19, 23, 24). It was recently demonstrated that laminar SS elicited enhanced cyclooxygenase-2 expression in ECs, which was dependent on p38 activation *via* $\alpha_5\beta_1$ integrin–mediated signaling downstream of PECAM-1 (17). However, the spatial and temporal control *via* MAPKs that are differentially activated by SS and their downstream targets that regulate the transcription of VCAM-1 *vs.* ICAM-1, especially as they link to ER stress–mediated signaling, are largely unknown.

The objective of the current study was to delve the signaling mechanism linking mechanosensing at the plasma membrane to an ER stress response that specifically modulates cytokine-induced VCAM-1 expression. Because p38 activity is known to play a role in mechanosignaling downstream of PECAM-1, we hypothesized that p38 activation controls the ER stress response to regulate TNF-α–stimulated up-regulation of VCAM-1 that is dependent upon the magnitude of SS. By examining flow-mediated signaling along a continuous monolayer of HAECs within a shear gradient, we revealed that PECAM-1–mediated mechanosignaling promotes sustained TNF-α–induced p38 phosphorylation under low SS, which facilitates nuclear translocation of XBP1s and, together with IRF-1, spatiotemporally regulates the expression of VCAM-1.

MATERIALS AND METHODS

The protocols for cell culture and characterization, exposure to SS, immunofluorescence imaging, and analysis are similar to those we have previously reported in Bailey *et al.* (7).

Cell culture and treatment protocol

HAEC (lot 2228, derived from a 21-yr-old female, and lot 7F4409 from a 34-yr-old male; Genlantis, San Diego, CA, USA) were expanded separately on culture flasks in Endothelial Growth Medium 2 (Lonza, Basel, Switerland) with a 1-time antibiotic-antimycotic solution (Thermo Fisher Scientific, Waltham, MA, USA) and used for experiments between passages 5 and 7. Because unstimulated HAECs express very low levels of VCAM-1 that are not significantly up-regulated by SS, cells were stimulated with TNF-α to observe the

modulatory effect of SS on inflammation. Each lot was characterized for a consistent dose response to TNF-α (R&D Systems, Minneapolis, MN, USA) stimulation by flow cytometry. HAECs were treated with 0.3 ng/ml TNF-α, corresponding to the EC_{50} for up-regulation of VCAM-1 or ICAM-1, in growth medium with 10% fetal bovine serum. Small molecule inhibitors were introduced to the medium for 1 h pretreatment before stimulating with TNF-α and SS for the following time periods indicated: p38 (SB203580; 10 μM; Cell Signaling Technology, Danvers, MA, USA), ERK1/2 (PD98059; 10 μM; Cell Signaling Technology), PI3K (LY294002; 30 μM; Cell Signaling Technology), or MAPK phosphatase 1 (MKP-1) (NSC 95397; 100 mM; Santa Cruz Biotechnology, Dallas, TX, USA).

Shear flow experiments

HAECs were exposed to fluid shear flow within a microfluidic chamber inspired by Hele-Shaw 2-dimensional stagnation flow theory and fabricated from polydimethylsiloxane using soft photolithography as previously described in refs. 8, 9, and 25. The channel width increases from the inlet to the outlet, generating a linearly decreasing magnitude of SS as a function of distance from the inlet and resulting in a stagnation point just proximal to the outlet. For a constant flow rate, the wall SS (τ_w) along the centerline of the channel changes linearly with axial distance (x) as follows:

$$\tau_w = \frac{6\mu \times Q}{h^2 \times w_1}\left(1 - \frac{x}{L}\right),$$

where μ is the viscosity of the flow medium, Q is the volumetric flow rate, h is the channel height, w_1 is the channel width at the inlet, and L is the length of the channel. HAECs were seeded on collagen type 1–coated (100 μg/ml; Thermo Fisher Scientific) glass coverslips and grown to 90–95% confluency. Polydimethylsiloxane microfluidic chambers were reversibly vacuum adhered to the HAEC monolayers. Leibovitz-15 medium (Thermo Fisher Scientific) supplemented with 10% fetal bovine serum, endothelial BulletKit (Lonza), and 1× antibiotic-antimycotic was used as flow medium to maintain pH in the absence of CO_2 regulation. A closed-loop flow system was powered by a Masterflex L/S Peristaltic Pump (Cole-Parmer, Vernon Hills, IL, USA) in a humidified chamber maintained at 37°C. To observe changes in CAM expression, HAECs were stimulated at a TNF-α concentration corresponding to the EC_{50} for CAM up-regulation (0.3 ng/ml) in the presence and absence of SS for 4 h. MAPKs, ER stress markers, and transcription factor activation were measured over 2 h of exposure.

Cell transfection

Lentivirus transduction particles (MilliporeSigma, Burlington, MA, USA) containing short hairpin RNAs (shRNAs) against PECAM-1 (TRCN0000057801) were introduced to HAECs at a multiplicity of infection of 2.5 for 12 h in medium and then diluted to a multiplicity of infection of 1.25 for another 36 h. Puromycin (MilliporeSigma) was added to the growth medium at 1 μg/ml for 48 h to select for transfected cells. The efficiency of knockdown was confirmed *via* Western blot to be >75%.

Immunofluorescence microscopy

Treated cells were rinsed in PBS and fixed in 4% paraformaldehyde (Electron Microscopy Sciences, Hatfield, PA, USA) for 10 min. Nonspecific binding was inhibited with 2% TruStain FcX (BioLegend, San Diego, CA, USA) in PBS before labeling with the following primary antibodies for 2 h: anticalreticulin (6468; 1:200; Santa Cruz Biotechnology), anti–VCAM-1 (555647; 1:10; BD Biosciences, San Jose, CA, USA), anti–ICAM-1 (322714; 1:20; BioLegend), anti-XBP1s (7160; 1:25; Santa Cruz Biotechnology), anti–phosphorylated (p)-p38 (9215; 1:100; Cell Signaling Technology), anti–IRF-1 (657602; 1:100; BioLegend), or anti–MKP-1 (271684 or 373841; 1:50; Santa Cruz Biotechnology). Fluorescently conjugated secondary antibodies applied in blocking buffer were chosen for their reactivity and emission properties. Primary mouse antibodies were stained with Alexa Fluor 555 goat anti-mouse (A21425; Thermo Fisher Scientific), primary goat antibodies were stained with Alexa Fluor 546 rabbit anti-goat (A21085; Thermo Fisher Scientific), and primary rabbit antibodies were stained with Alexa Fluor 647 goat anti-rabbit (A21245; Thermo Fisher Scientific), each diluted to 1:500 in blocking buffer. To detect intercellular proteins, 0.1% Triton X-100 (MilliporeSigma) was added to blocking buffers and staining buffers. Immunolabeled samples were mounted using Vectashield with DAPI (Vector Laboratories, Burlingame, CA, USA) or ProLong Gold with DAPI (Thermo Fisher Scientific). Cell surface proteins (VCAM-1 and ICAM-1) were imaged using a Nikon inverted microscope (Nikon, Tokyo, Japan) equipped with a 16-bit Zyla sCMOS camera (Oxford Instrumentals, Abingdon, United Kingdom) and a ×60 objective (numerical aperture, 1.49; Nikon). Images were captured using 4 × 4 binning (2.33 pixels/μm resolution). Intracellular protein targets (p38, XBP1, IRF-1, and MKP-1) were captured using a confocal laser scanning microscope (FV1000; Olympus, Tokyo, Japan). For each flow experiment, 5 representative images were captured at each SS magnitude corresponding to a fixed axial position within the flow chamber, such that they deviated from the expected SS by <0.2 dyn/cm^2. These images were quantified using ImageJ (National Institutes of Health, Bethesda, MD, USA). From the images, DAPI nuclear staining was used to identify >60 individual cells in total. Quantification of nuclear *vs.* cytoplasmic staining varied by protein target as reported in the text. A mean fluorescence intensity for the ~60 individual cells yielded a single value per SS magnitude per flow run. Typically, 3–5 experiments were used to report the variance observed in these studies. A previous study using calibration beads demonstrated a direct correlation between fluorescence intensity measured on chips in this manner and receptor numbers per cell by flow cytometry (26).

ER morphology

HAECs were exposed to TNF-α and SS for 2 h, immunolabeled for the ER resident protein calreticulin, and imaged by confocal laser scanning microscopy (FV1000; Olympus). To block p38 activation, cells were preincubated with SB203580 for 1 h prior to costimulation with SS and TNF-α. ER expansion (associated with a state of ER stress) was measured by calculating the coefficient of variation of cytoplasmic calreticulin pixel intensity, which increases with increasing spatial heterogeneity (7, 27).

Statistical analysis

Data were analyzed using Prism software v.5.02 (GraphPad, La Jolla, CA, USA). A Student's t test was used to compare 2 experimental groups at a given SS or time point or to assess the effect of treatment comparing high and low SS. Two-tailed values of $P < 0.05$ were considered statistically significant unless otherwise indicated.

RESULTS

VCAM-1 and ICAM-1 expression on inflamed HAECs is regulated by SS

To investigate how the magnitude of SS is sensed to affect the spatial regulation of VCAM-1 and ICAM-1 expression by inflamed endothelium, a vascular mimetic microfluidic chamber was employed that applies a linear gradient of fluid SS across a monolayer of HAECs (7–9). To stimulate transcriptional up-regulation of adhesion receptors, a low dose of TNF-α (0.3 ng/ml, the EC_{50} for CAM up-regulation) was added to the flow media that elicited a robust inflammatory response characterized by a reproducible pattern of CAM expression (7, 8). VCAM-1 and ICAM-1 were quantified *via* immunofluorescence microscopy along the monolayer (**Fig. 1*A***). Antibody detection of CAMs in the absence of cytokine stimulation was indistinguishable from the labeling of unstimulated HAECs with nonspecific isotype control antibodies (Fig. 1*B*, *C*, dashed lines). Stimulation with TNF-α for 4 h increased VCAM-1 expression by 2-fold in HAECs at the near 0–flow rate stagnation point, which provides an internal control for calibrating expression changes within a monolayer that closely align with observations made in static culture (7). At a position

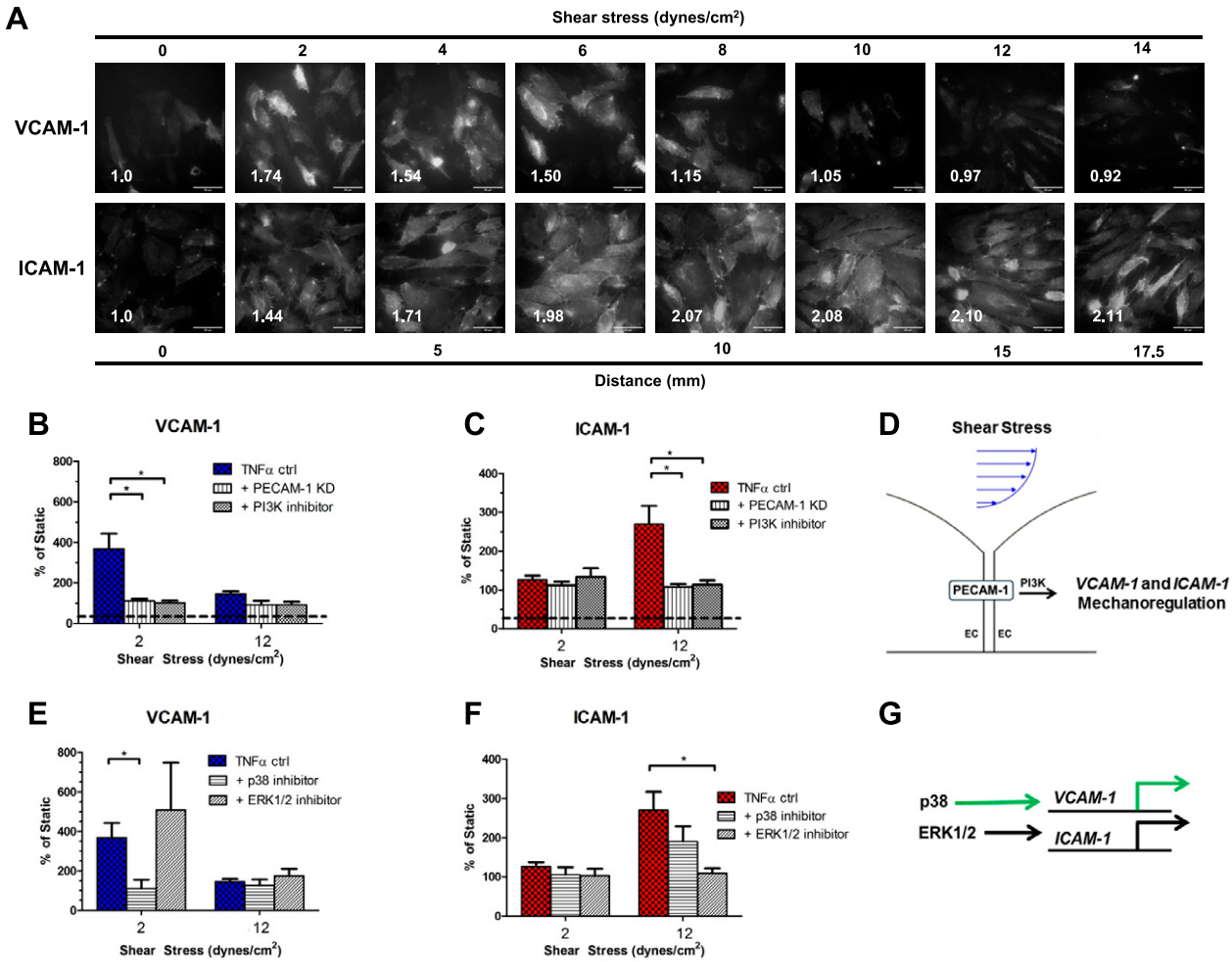

Figure 1. VCAM-1 and ICAM-1 expression on inflamed HAECs is regulated by SS. HAEC monolayers were exposed to TNF-α (0.3 ng/ml) and a fluid SS gradient (0–16 dyn/cm^2 over 20 mm) for 4 h in a Hele-Shaw microfluidic device. Cells were immunolabeled for VCAM-1 and ICAM-1 protein and images were captured by fluorescence microscopy. *A*) Representative imaging series for VCAM-1 and ICAM-1 captured at discrete SS levels within a single monolayer. Fold changes for each SS level in this image series expressed relative to 0 dyn/cm^2 (static point). Scale bars, 50 μm. *B, C*) VCAM-1 (*B*) and ICAM-1 (*C*) were quantified over multiple experiments and expression was compared at representative low- (2 dyn/cm^2) and high- (12 dyn/cm^2) SS levels corresponding to the maximum reproducible change in TNF-α–stimulated VCAM-1 expression. Dashed lines represent initial (static, untreated) intensities. A role for PECAM-1–mediated mechanotransduction was assessed using PECAM-1–deficient cells generated by stable lentiviral transfection of shRNA. PI3K was blocked with the small molecule inhibitor LY294002. *D*) Summary schematic illustrating common PECAM-1–dependent mechanosignaling to both VCAM-1 and ICAM-1. *E, F*) VCAM-1 (*E*) and ICAM-1 (*F*) were quantified as above using a small molecule inhibitor to p38 (SB203580) or ERK1/2 (PD98059). *G*) Schematic highlighting unique MAPK-signaling dependence of CAM expression. Values are means ± SE; n = 3–5 experiments. *$P < 0.05$.

along the gradient of SS corresponding to 2 dyn/cm^2, VCAM-1 expression rose to its peak level, increasing by an additional 2.5–3-fold from the stagnation point. Further along the gradient, VCAM-1 expression dropped continuously back to static levels at the high SS of 12 dyn/cm^2 (Fig. 1*B*). In contrast, ICAM-1 expression continuously rose to its peak level, more than doubling expression from the static baseline at 12 dyn/cm^2 (Fig. 1*C*). VCAM-1 expression continued to trend downward, whereas ICAM-1 expression plateaued at peak levels beyond 12 dyn/cm^2. However, the narrowest part of the chamber nearest the entrance does not routinely contain sufficient cells to be quantifiable, particularly with more poorly expressed intracellular targets. Significant changes in CAM expression were consistently observed when comparing 2 and 12 dyn/cm^2 as they changed relative to the static condition. These low- and high-SS magnitudes, respectively, correspond to approximate time average values associated with sites of susceptibility and resistance to atherosclerosis in arteries. These SS levels thus constitute an important reference for significant changes in inflammatory CAM expression and motivate our focus on this comparison throughout the manuscript.

We next examined the signal pathways responsible for SS-mediated differential expression between VCAM-1 and ICAM-1. PECAM-1 is known to mechanotransduce signals derived from fluid SS *via* the downstream kinase PI3K (17). Employing shRNA-loaded lentivirus to knock down PECAM-1, transfected HAECs were confirmed to be 75–80% deficient in PECAM-1 protein by Western blot as previously reported in Bailey *et al*. (7). PECAM-1–deficient HAECs lost the capacity to significantly increase expression of VCAM-1 and ICAM-1 from cytokine-stimulated levels with exposure to SS, indicating a loss of mechanosensing. Employing a small molecule inhibitor to PI3K also abrogated up-regulation in CAM expression with SS (Fig. 1*B, C*). These data confirmed the importance of SS-mediated mechanotransduction, sensed by PECAM-1 and signaled *via* PI3K, in the regulation of TNF-α–induced CAM expression, but did not provide insight into the differential regulation observed at high *vs.* low SS (Fig. 1*D*).

Because ERK1/2 and p38 expression are up-regulated by TNF-α and their activity is elevated downstream of PECAM-1-PI3K mechanosensing (17, 23), we examined their role in the differential regulation of VCAM-1 and ICAM-1 expression by pretreating HAECs with small molecule inhibitors of these MAPKs (Fig. 1*E, F*). The p38 inhibitor SB203580 had a potent (70%) inhibitory effect on the SS-dependent rise to maximum VCAM-1 expression at 2 dyn/cm^2 but no effect at high SS (Fig. 1*E*). In contrast, p38 inhibition did not significantly decrease the SS-dependent rise to maximum ICAM-1 expression at 12 dyn/cm^2 (Fig. 1*F*). Conversely, the ERK1/2 inhibitor PD98059 had no significant effect on maximum VCAM-1 expression at low SS but significantly reduced the peak in ICAM-1 at high SS by 59%. These data reveal distinct roles for the 2 arms of MAPK regulation of CAM expression at the high *vs.* low SS for ICAM-1 and VCAM-1, respectively (Fig. 1*G*).

Phosphorylation of p38 is enhanced by low SS to activate nuclear transport of XBP1 and IRF-1

To investigate the mechanism by which signaling through PECAM-1 superposes with the ER stress response in transcriptional regulation of VCAM-1 production, we measured the activation kinetics of p38 along with the transcription factors XBP1 and IRF-1 as a function of position in the flow channel and over the time course of TNF-α stimulation. Because these intracellular targets provided weaker signals for immunofluorescence detection relative to the highly expressed CAMs, we applied confocal imaging to quantify nuclear expression of p-p38, XBP1s, and IRF-1 proteins. On average this resulted in small albeit consistent changes in signal as a function of SS (*e.g.*, **Fig. 2*A***), which were significant when comparing expression at 2 and 12 dyn/cm^2 that registered the largest changes in VCAM-1 expression. In terms of expression modulation with time along the channel, under static conditions, p-p38 rose steadily over the initial 30 min of TNF-α stimulation, peaking at more than double that of unstimulated samples before dropping back toward the baseline level at 1 h (Fig. 2*B*). In the presence of shear flow, p-p38 peaked at comparable levels to the TNF-α static condition and rose similarly under low or high SS. A significant difference was observed in the level of nuclear p-p38 at 2 h, which dropped more steeply under high SS (to ~20% below baseline unstimulated) compared with low SS (which remained elevated by 56%).

The rise in nuclear XBP1s in TNF-α-stimulated HAECs was slower than that of p-p38 over the initial 60 min (Fig. 2*C*). Under static and high-SS conditions, XBP1s rose ~24%, whereas XBP1s signal in low-SS samples rose by 48% above untreated at 60 min and remained significantly elevated at this level, coinciding with peak p-p38. Over this time, XBP1s expression in static and high-SS samples tracked within 20% of unstimulated. To determine if the ER stress response mediated by the rise in XBP1 affected IRF-1, which promotes VCAM-1 transcription, we measured the kinetics of IRF-1 expression in the nucleus (Fig. 2*D*). In TNF-α–stimulated HAECs, IRF-1 expression rose commensurate with XBP1 and at a higher rate in the presence of SS. At low SS, expression increased to a peak by 60 min and remained elevated up to 2 h, coinciding with the period of elevated p38 and XBP1 activity. Over this duration, the high-SS and static samples tracked together significantly lower at levels equivalent to unstimulated. Taken together, the kinetics reveal that sustained p-p38 activity under low SS may provide a signaling mechanism for amplification of VCAM-1 through promoting the increased nuclear transport of XBP1 and IRF-1.

SS sustains phosphorylation of p38 following TNF-α stimulation

To delve into the role of PECAM-1 mechanotransduction in activation of p38, we quantified nuclear localization of

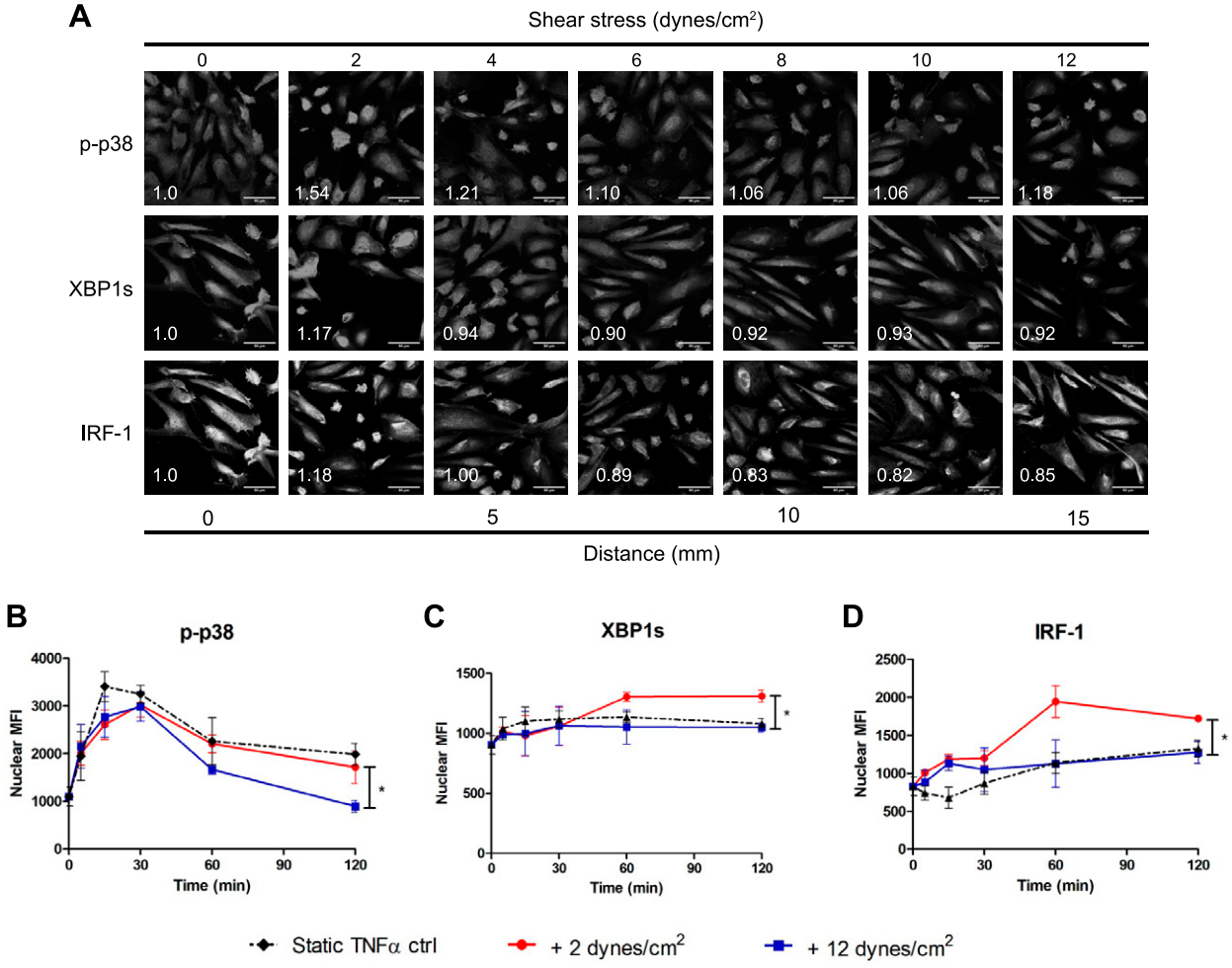

Figure 2. Sustained p38 activation under low SS is accompanied by delayed activation of XBP1 and IRF-1. HAEC monolayers were exposed to TNF-α (0.3 ng/ml) and a fluid SS gradient (0–16 dyn/cm^2 over 20 mm) for 5–120 min in a Hele-Shaw microfluidic device. Cells were immunolabeled for p-p38, XBP1s, or IRF-1, and images were captured by confocal microscopy. *A*) Representative imaging series for each target captured at discrete SS levels within a monolayer at 120 min. Fold changes for each SS level in this image series expressed relative to 0 dyn/cm^2 (static point). Scale bars, 50 μm. *B–D*) Nuclear p-p38 (*B*), XBP1s (*C*), and IRF-1 (*D*) expression over time were quantified over multiple experiments and expression was compared at representative low- (2 dyn/cm^2) and high- (12 dyn/cm^2) SS levels corresponding to the maximum reproducible change in TNF-α–stimulated VCAM-1 expression. MFI, mean fluorescence intensity. Values are means ± SE; n = 3–6 experiments. *$P < 0.05$.

p-p38 across the gradient of SS at time points corresponding to its peak (30 min) and sustained (2 h) activity in control and PECAM-1–deficient HAECs. In the absence of TNF-α, sheared HAECs exhibited no increase in p-p38 translocation from static, unstimulated levels at either time point (corresponds to dashed line in **Fig. 3*A***). At 30 min, PECAM-1–deficient cells exhibited a comparable peak in p-p38 to the TNF-α-stimulated control HAECs, neither of which differed with SS magnitude. In contrast, a significant drop in p38 activation was observed comparing low and high SS–treated HAECs at 2 h (Fig. 3*A, B*). This differential p-p38 activity was not observed in PECAM-1–deficient HAECs. Thus, blocking PECAM-1 mechanotransduction abrogated the sustained activation of p38 at 2 dyn/cm^2. Together, these data confirm that although the early peak in p38 activation was attributable mainly to TNF-α stimulation, sustained and differential activation was regulated by the magnitude of SS.

MKP-1 regulates the SS-mediated phosphorylation of p38

The kinetics of p38 activation and its nuclear transport that is up-regulated by atherosusceptible low levels of SS led us to investigate the role of phosphatases in its regulation. HAECs were pretreated with either a small molecule inhibitor or activator of p38 introduced to the flow medium after 30 min of SS, which coincided with the peak in TNF-α–stimulated activity. SB203580, a steric inhibitor of p38 phosphorylation, did not alter the level of nuclear p-p38 following 2 h of low SS but nominally increased activity at the high SS (**Fig. 4*A***). In contrast, activation of p38 by pretreatment with anisomycin significantly increased nuclear p-p38 at both 2 and 12 dyn/cm^2. Alternatively, inhibition of MKP-1 that acts on p38 with NSC 95397 led to a significant increase in nuclear p-p38 at high SS and exerted an insignificant increase at low SS.

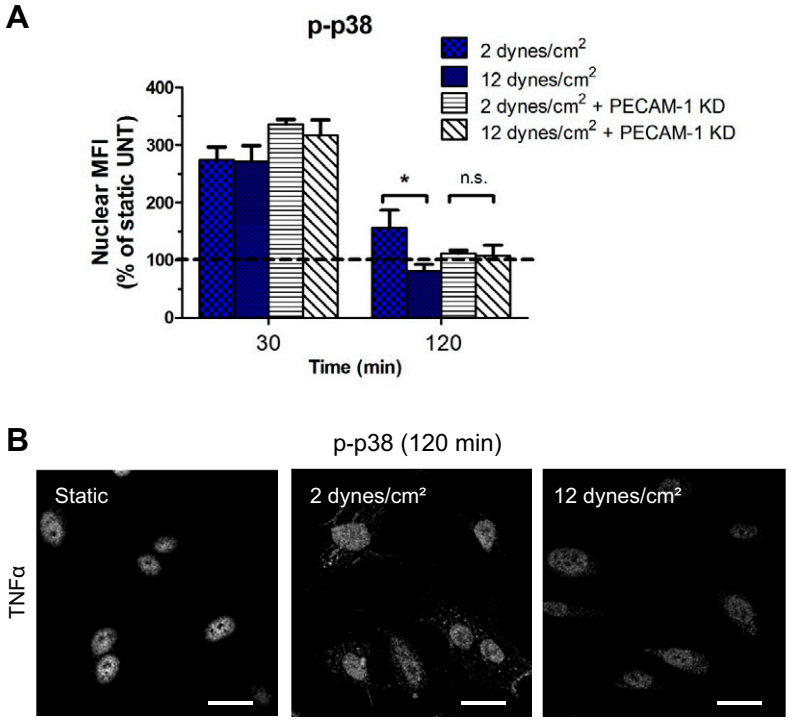

Figure 3. SS sustains phosphorylation of p38 following TNF-α stimulation. HAEC monolayers were exposed to TNF-α (0.3 ng/ml) and a fluid SS gradient in a Hele-Shaw microfluidic device. *A*) A role for PECAM-1–mediated mechanotransduction was assessed at time points corresponding to peak (30 min) and sustained (120 min) nuclear p38 activity in control and PECAM-1–deficient (shRNA) HAECs. Dashed line represents initial (static, untreated) intensity. Values are means ± SE; $n = 3$–6 experiments. $^*P < 0.05$. *B*) Representative confocal images captured at discrete SS levels coinciding with the SS-dependent difference in p-p38 expression observed at 120 min. Scale bars, 30 μm. MFI, mean fluorescence intensity.

For MKP-1 to abrogate the mechanoregulation of p-p38, we hypothesized that its expression could also be regulated by SS. We next quantified changes in its expression in TNF-α–stimulated HAECs along the SS gradient at 45 min, a time point corresponding to the peak in p38 dephosphorylation (*e.g.*, Fig. 4*B*). Cytoplasmic MKP-1 expression was significantly higher (26%) along the HAEC monolayer at the position of high SS compared with the low-SS region (Fig. 4*C, D*). This differential regulation of MKP-1 activity was normalized to static levels in PECAM-1–deficient HAECs. These data suggest that the MKP-1 phosphatase activity is suppressed at low SS and promoted at high SS, resulting in sustained p38 activation during inflammatory stimulation (Fig. 4*E*).

p-p38 promotes nuclear localization of IRF-1 that promotes VCAM-1 transcription

To determine the target of p38 activation in ER stress–mediated regulation of VCAM-1 expression, we assessed ER morphologic expansion and XBP1 expression that is a product of the UPR. Low SS elicited ER expansion, consistent with its ability to enhance ER stress in TNF-α–stimulated HAECs (**Fig. 5*A***). Treatment with the p38 inhibitor SB203580 did not significantly affect ER morphology in comparing the low- *vs.* high-SS regions, suggesting that the effects of p-p38 on VCAM-1 expression occur downstream of the ER stress response and motivating examination at the level of the UPR effectors.

We next investigated a role for p-p38 in stabilizing XBP1s for its nuclear translocation by quantifying nuclear XBP1s levels while manipulating the level of p-p38 activation in TNF-α–stimulated HAECs. Nuclear XBP1s mirrored the mechanoregulation pattern of p-p38 in that it was unchanged by inhibition with SB203580 but enhanced by the agonist anisomycin at both 2 and 12 dyn/cm^2, respectively (Fig. 5*B*). Notably, the MKP-1 inhibitor NSC 95397 elicited a 41% increase in XBP1s, which coincided with the increase in p-p38 at high SS. These results are consistent with enhanced MKP-1 activity under high SS suppressing p38 and XBP1 activity compared with low SS. To determine if the greater level of p-p38 activity elicited at low SS functioned to enhance XBP1s activity in this region of the flow channel, we measured its rise in HAEC monolayers treated with the p38 inhibitor during TNF-α stimulation. In the presence of p38 inhibition with SB203580, nuclear transport of XBP1s was reduced to baseline static levels that were equivalent at low and high SS (Fig. 5*C, D*). We conclude that the nuclear translocation of XBP1s is dependent upon the availability of p-p38 that is mechanoregulated and located downstream of TNF-α–stimulated ER stress.

The potent induction of the ER stress response at atherosusceptible regions of low SS results in elevated production of XBP1s that culminates in enhanced IRF-1 expression that promotes VCAM-1 transcription and elevated expression. We next confirmed that p-p38–dependent nuclear transport of XBP1s is a mechanism that links mechanoregulation with an increase in nuclear IRF-1. HAECs were pretreated with the p38 inhibitor SB203580 in the presence of shear flow and TNF-α stimulation and the effect of low SS on enhancing IRF-1 nuclear translocation was reduced to static levels (Fig. 5*E, F*). Furthermore, nuclear IRF-1 was not significantly altered within the region of high SS by p38 inhibition. We conclude that the activation of p38 exerts its effects on IRF-1–mediated increase in VCAM-1 because of its capacity to increase nuclear transport of XBP1s as a function of the magnitude of SS sensed *via* PECAM-1.

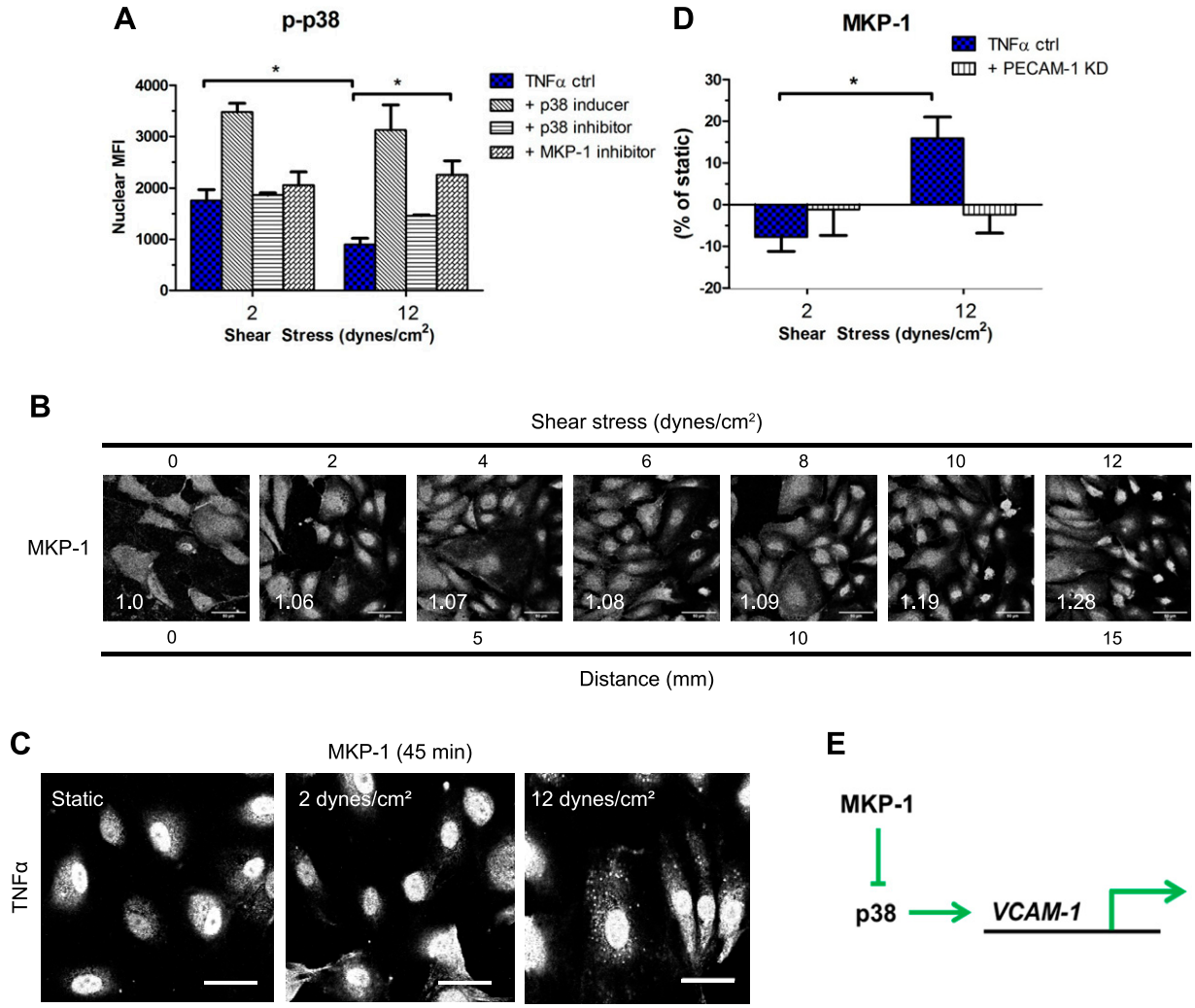

Figure 4. MKP-1 regulates the SS-mediated phosphorylation of p38. HAEC monolayers were exposed to TNF-α (0.3 ng/ml) and a fluid SS gradient in a Hele-Shaw microfluidic device for 2 h. After 30 min of treatment, p38 agonist (anisomycin), p38 inhibitor (SB203580), or MKP-1 inhibitor (NSC 95397) was added to the flow medium. *A*) Nuclear p-p38 was quantified from confocal images. *B*) MKP-1 expression was quantified from confocal images in HEACs treated with TNF-α and exposed to the SS gradient. Representative imaging series for MKP-1 captured at discrete SS levels within a monolayer at 45 min. Fold changes for each SS level in this image series expressed relative to 0 dyn/cm^2 (static point). Scale bars, 50 μm. *C*) Cytoplasmic MKP-1 expression was quantified over multiple experiments and expression was compared at discrete SS levels coinciding with the SS-dependent difference in p-p38 expression. Representative images: scale bars, 35 μm. *D*) A role for PECAM-1–mediated mechanotransduction was assessed in control and PECAM-1–deficient (shRNA) HAECs. *E*) Schematic illustrating the regulation of p38 by MKP-1 to control VCAM-1 expression. MFI, mean fluorescence intensity. Values are means ± SE; n = 3–6 experiments. *$P < 0.05$.

DISCUSSION

The arterial endothelium senses mechanical forces imparted by the flow of blood and transduces these into biochemical signals to drive pathways that locally regulate inflammation. Notable in regard to focal atherosclerosis is the spatial regulation of VCAM-1 expression, which maps to arterial regions of low SS that exhibit a propensity for plaque formation in humans and mice (2–6). The current study applied microfluidic artery-on-a-chip technology to produce a physiologically relevant gradient in fluid SS with magnitudes ranging from those considered atherosusceptible to atheroprotective over a single monolayer of HAECs. This enabled the spatial assessment of PECAM-1–regulated pathways that mechanotransduce differential CAM expression in response to low-dose TNF-α stimulation. We report that at relatively low-magnitude SS, PECAM-1–mediated mechanosignaling promoted sustained p38 phosphorylation, which was dependent on a reduction in MKP-1. Enhanced p38 activity, in turn, potentiated a cytokine-induced ER stress response by promoting stabilization and nuclear translocation of XBP1s where, together with enhanced IRF-1 activity, it promoted maximal VCAM-1 expression that supports efficient monocyte recruitment (**Fig. 6**).

Inflammatory stimuli that promote atherosclerosis such as the cytokine TNF-α, dietary lipoproteins, and pathogens induce EC up-regulation of CAMs (2). HAECs are normally relatively resistant to inflammation in that they express CAMs at low levels in the absence of stimulation that are not significantly up-regulated by SS alone. In contrast, stimulation with TNF-α elicits a predictable

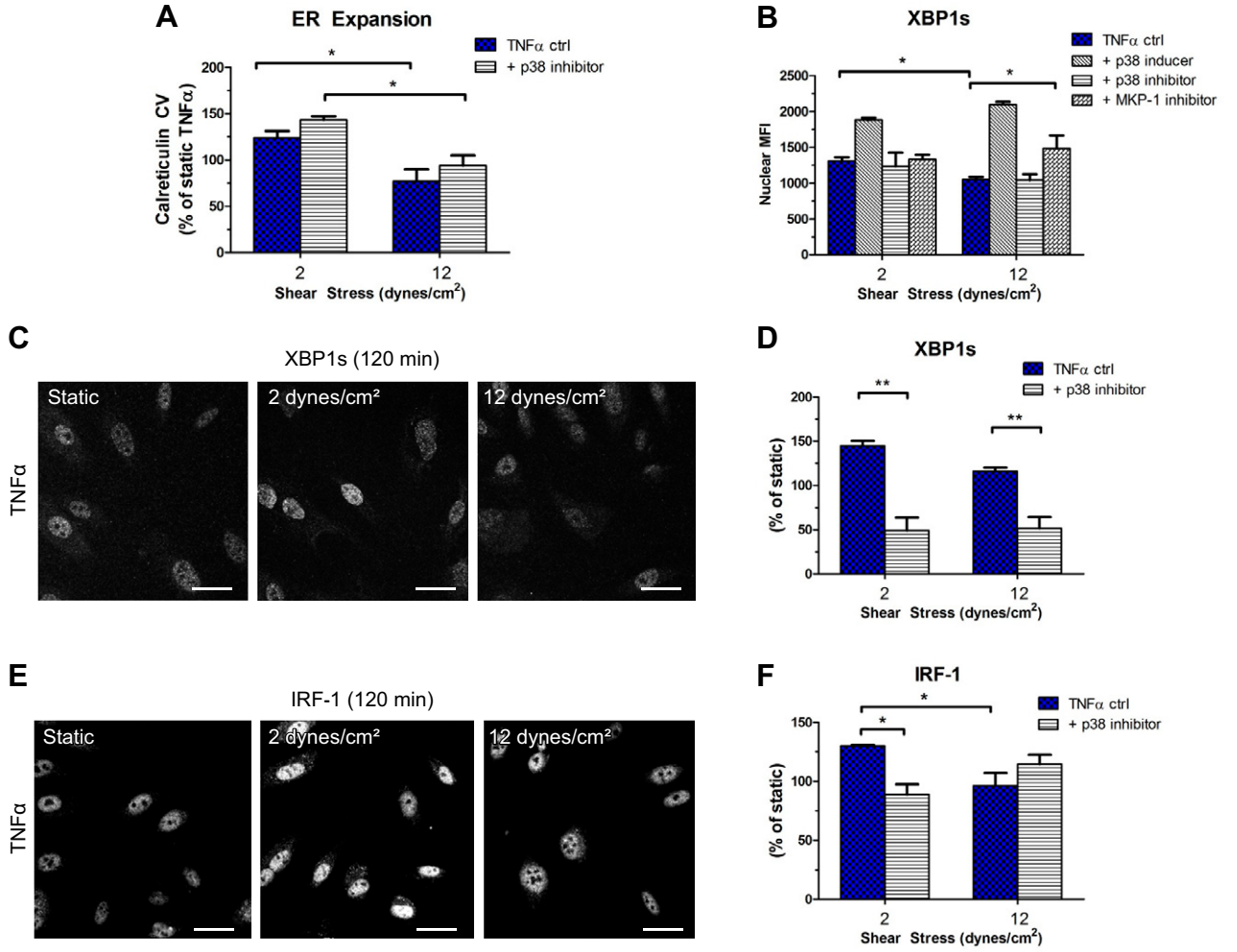

Figure 5. p-p38 promotes nuclear localization of IRF-1 that promotes VCAM-1 transcription. HAEC monolayers were exposed to TNF-α (0.3 ng/ml) and a fluid SS gradient in the presence or absence of p38 inhibitor (SB203580). *A*) Expression of the ER resident protein calreticulin was imaged by confocal immunofluorescence microscopy and used to calculate a metric of ER expansion. *B*) After 30 min of SS and TNF-α exposure, p38 inducer (anisomycin), p38 inhibitor (SB203580), or MKP-1 inhibitor (NSC 95397) was added to the flow medium and nuclear XBP1s was quantified from confocal images at 120 min. *C*) A role for mechanoregulation of XBP1s activity by p38 was assessed in the presence or absence of p38 inhibition over the entire 120 min of treatment. Representative confocal images captured at discrete SS levels coincide with the SS-dependent difference in p-p38 expression. Scale bars, 30 μm. *D*) Nuclear XBP1s quantified over multiple experiments. *E*) IRF-1 activity was assessed in the presence or absence of p38 inhibition over the entire 120 min of treatment. Representative confocal images captured at discrete SS levels coinciding with the SS-dependent difference in p-p38 expression. Scale bars, 30 μm. *F*) Nuclear IRF-1 quantified over multiple experiments. CV, coefficient of variation; MFI, mean fluorescence intensity. Values are means ± SE; $n = 3$–6 experiments. $^*P < 0.05$, $^{**}P < 0.005$.

inflammatory response, characterized by up-regulation of multiple CAMs, which are significantly and differentially modulated by the magnitude of SS (9). In particular, the level of VCAM-1 expression elicited by TNF-α is suppressed by high SS but is greatly enhanced by low atherosusceptible levels of SS. In this manner, HAECs within our flow channel exhibit spatial mechanoregulation of an inflammatory stimulus on a scale of millimeters, which is similar to the sort of abrupt transitions in wall SS that can occur at atherosusceptible sites such as the aortic arch. We showed that enhanced expression of VCAM-1 is dependent upon the increased nuclear expression and activity of IRF-1 that promotes its transcription (7, 8). Moreover, low SS was synergistic with TNF-α in eliciting a potent ER stress response that promoted maximal IRF-1–dependent VCAM-1 expression. In contrast, during inflammation, the expression of ICAM-1 increases in direct proportion to the magnitude of SS, and its transcriptional regulation is independent of ER stress (7, 9). Because SS alone did not up-regulate markers of UPR (7), the question remained as to how signaling *via* mechanotransduction commensurate with the magnitude of SS superposed with that induced by TNF-α to modulate VCAM-1 activity.

The mechanosignaling mechanisms that govern the precise spatial regulation of acute inflammatory responses by endothelium that underlie focal atherosusceptibility are not completely understood. Mechanotransduction of SS potentially involves an integrated response sensed through a host of membrane-spanning molecules. Among these, PECAM-1 is recognized as a primary force transducer

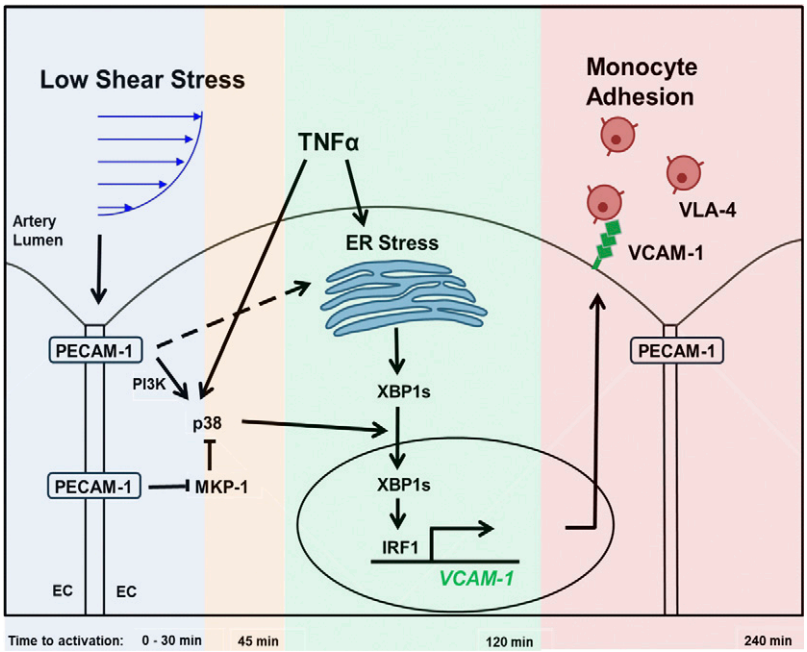

Figure 6. Summary schematic illustrating the mechanoregulation of p38 activity to enhance cytokine-induced, ER stress–mediated VCAM-1 expression by atherosusceptible low SS. Background shading corresponds to timeline for events leading to the maximum activation of cytokine and SS-induced inflammation. VLA-4, very late antigen-4.

that plays a central role in initiating flow-induced signaling (15–17). We reported that the shear modulation of both VCAM-1 and ICAM-1 in TNF-α-stimulated HAEC was dependent upon a PECAM-1-mediated mechanism (7). However, these adhesion receptors display very different patterns of expression within a shear gradient. In the case of VCAM-1 specifically, we showed that an ER stress response involving XBP1 and eIF2α was increased by low SS in TNF-α–stimulated HAECs downstream of PECAM-1 activation (7). Here, we aimed to delve into the mechanism by which SS can affect signaling that converges on the ER to modulate the specificity of this response. We first showed that inhibition of PI3K downstream of PECAM-1 abrogated mechanoregulation of both TNF-α–stimulated VCAM-1 and ICAM-1 expression. This broad inhibition is consistent with our previous study and others reporting that either knockdown of PECAM-1 or PI3K significantly inhibited other shear-modulated functions mediated by integrins and MAPKs (7, 15–17). We conclude that the specificity in mechanoregulation of VCAM-1 lies downstream of the PECAM-1 transduction complex and involves kinase phosphorylation to modulate the dynamics of this inflammatory response.

We investigated signaling at the level of MAPKs to explain the differential patterns of VCAM-1 and ICAM-1 expression as a function of SS magnitude. Previous studies have typically focused on the response to laminar flow producing relatively high-magnitude SS (19, 20). For example, Berk *et al.* and others have reported on the opposing roles for SS-activated MAPKs ERK1/2 and p38, with the former characterized as progrowth and antiapoptotic and the latter as proinflammatory and proapoptotic (18, 28). Here, we demonstrate that the pattern of SS-modulated VCAM-1 expression in inflamed HAECs was uniquely dependent upon p38 activity, whereas ICAM-1 was dependent on ERK1/2. The association of ERK1/2 in signaling elevated ICAM-1 expression at high SS is a novel finding that warrants further investigation because it may further activate known or heretofore undefined transcription factors that confer atheroprotective responses. Because p38 activity specifically mapped to enhanced VCAM-1 at low-SS magnitude associated with sites of atherosusceptibility, we investigated its spatial and temporal regulation under shear flow.

Previous studies demonstrated that p38 is rapidly and transiently activated by the onset of laminar flow or cytokine stimulation (19, 20, 22). Here, we observed that p38 activation peaked within 30 min of TNF-α stimulation and this activation was not a function of SS magnitude. In contrast, deactivation of p38 occurred more rapidly in HAECs exposed to high SS, leading to differential activity levels at 2 h. This response was attributable to enhanced early expression of MKP-1 under high SS. Although there is evidence in the literature supporting p38 activation by SS and TNF-α, less is known regarding how SS-modulated p38 signaling affects downstream targets to modulate VCAM-1 transcription (17, 19, 23, 24). Several reports in animal models link SS modulation of p38 to regulation of VCAM-1. Yamawaki *et al.* (24) demonstrated that blocking p38 in a rabbit artery perfusion model inhibited TNF-α–induced VCAM-1 expression. Zakkar *et al.* (29) demonstrated that the dephosphorylation of p-p38 *via* the phosphatase MKP-1 was associated with atheroprotective regions of the mouse aorta. Upon deleting MKP-1 with RNA interference, they demonstrated a significant increase in VCAM-1. Moreover, in these protected regions, activity of the transcription factor nuclear factor erythroid 2-related factor 2 negatively regulated p38-dependent VCAM-1 expression, and this suppression was attributed, in part, to enhanced activity of MKP-1 (30). These studies support the *in vivo* relevance of our findings, revealing the dynamic MKP-1–dependent regulation of p38 phosphorylation that is activated by PECAM-1 mechanotransduction

and regulates transcriptional activity as a function of the magnitude of SS in human cells.

We investigated how enhanced activation of p38 could act to modulate an ER stress response that promotes VCAM-1 expression. Inhibition of p38 did not elicit measurable morphologic changes in the ER induced by TNF-α or SS. This suggested that SS-modulated p38 could be acting downstream to enhance an ER stress response through 1 or more elements of the UPR. Active p38 was recently shown to phosphorylate XBP1s at Thr48 and Ser61, dramatically increasing its localization to the nucleus in livers of diabetic mice (31). We proposed that a similar mechanism could explain the enhancement of ER stress–induced VCAM-1 by low SS. We demonstrate that nuclear XBP1s follows the peak in p38 activation and that p38 inhibition further prevented XBP1s nuclear localization. Finally, by blocking the peak in p38 activity, we observed that nuclear IRF-1 necessary for maximal VCAM-1 transcription at low SS was normalized to static levels. Consistent with previous findings, we conclude that XBP1s plays a central role in promoting VCAM-1 through regulation of the stability of nuclear IRF-1 (7).

Absent of the ability to directly access human arteries, the Hele-Shaw microfluidic chamber applied here constitutes an artery-on-a-chip approach that enables the study of the earliest changes in EC and monocytes that promote atherosclerosis. The chamber mimics essential attributes of sites susceptible to atherosclerosis in arteries, including a physiologic range of SS that changes over a gradient that correlates closely with atherogenesis. We have established using this *ex vivo* model that the level of VCAM-1 expression by inflamed HAECs correlates strongly with enhanced recruitment of intermediate or inflammatory monocytes ($CD14^+/CD16^+$) from the blood, outcomes of functional relevance to the disease process (26). However, any rigid chamber geometry is limited in its capacity to fully reproduce the complexity of disturbed flow in arteries. Notably, flow reversal or oscillation may be an important contributor to atherosusceptibility *in vivo*. In previous studies, we demonstrated that SS magnitude was the most important flow attribute driving the mechanisms leading to the acute regulation of VCAM-1 studied here, which were relatively insensitive to oscillation or steepness of the gradient (7–9). A second limitation of the current study is the use of pharmacological inhibitors or shRNAs to inhibit pathways, which could potentially have nonspecific effects. Although we cannot rule out these effects, we applied inhibitors used effectively in previous studies and included the controls in our study to verify protein knockdown (17). Additional studies will be needed to verify the mechanism elucidated here *in vivo*.

In summary, this study elucidates a mechanism by which SS sensitizes the endothelium to a cytokine-induced ER stress response to spatially modulate inflammation. Divergence in signaling at the level of MAPK activation governed differential CAM expression along a gradient of fluid SS in a continuous monolayer of ECs. Dynamic regulation of p38 activity through differential activation of MKP-1 provided the first mechanistic link between PECAM-1–mediated mechanotransduction of SS and ER stress–mediated VCAM-1 expression. These data may in part explain the regulation of the atherosusceptible endothelial phenotype. In light of growing interest in the relationship between chronic ER stress and metabolic dysregulation in atherogenesis, these novel mechanistic insights may help identify targets for therapeutic intervention of atherosclerosis. FJ

ACKNOWLEDGMENTS

The authors thank Dr. Drew E. Glaser (Dr. Steven C. George Laboratory, University of California–Davis) for assistance with confocal imaging. This study was supported by the U.S. National Institute of Health (NIH) National Heart, Lung, and Blood Institute (Grant HL082689 to S.I.S. and A.G.P.) and the NIH National Institute of Allergy and Infectious Diseases (Grant AI047294 to S.I.S.). Research in the F.G.H. laboratory was funded by NIH National Institute of Diabetes and Digestive and Kidney Diseases Grant RO1DK095359 and NIH National Institute of Environmental Health Sciences Grant P42 ES04699. The authors declare no conflicts of interest.

AUTHOR CONTRIBUTIONS

K. A. Bailey conducted the experiments and prepared the figures; E. Moreno contributed to image acquisition and analysis; K. A. Bailey, S. I. Simon, and A. G. Passerini wrote the manuscript; and all authors consulted on experimental design, data analysis and interpretation, and edited the final manuscript.

REFERENCES

1. Benjamin, E. J., Blaha, M. J., Chiuve, S. E., Cushman, M., Das, S. R., Deo, R., de Ferranti, S. D., Floyd, J., Fornage, M., Gillespie, C., Isasi, C. R., Jiménez, M. C., Jordan, L. C., Judd, S. E., Lackland, D., Lichtman, J. H., Lisabeth, L., Liu, S., Longenecker, C. T., Mackey, R. H., Matsushita, K., Mozaffarian, D., Mussolino, M. E., Nasir, K., Neumar, R. W., Palaniappan, L., Pandey, D. K., Thiagarajan, R. R., Reeves, M. J., Ritchey, M., Rodriguez, C. J., Roth, G. A., Rosamond, W. D., Sasson, C., Towfighi, A., Tsao, C. W., Turner, M. B., Virani, S. S., Voeks, J. H., Willey, J. Z., Wilkins, J. T., Wu, J. H., Alger, H. M., Wong, S. S., and Muntner, P.; American Heart Association Statistics Committee and Stroke Statistics Subcommittee. (2017) Heart disease and stroke statistics-2017 update: a report from the American Heart Association. *Circulation* **135**, e146–e603; erratum: e646; 136, e196
2. Davies, P. F. (1995) Flow-mediated endothelial mechanotransduction. *Physiol. Rev.* **75**, 519–560
3. Glagov, S., Zarins, C., Giddens, D. P., and Ku, D. N. (1988) Hemodynamics and atherosclerosis. Insights and perspectives gained from studies of human arteries. *Arch. Pathol. Lab. Med.* **112**, 1018–1031
4. Libby, P. (2002) Inflammation in atherosclerosis. *Nature* **420**, 868–874
5. Mestas, J., and Ley, K. (2008) Monocyte-endothelial cell interactions in the development of atherosclerosis. *Trends Cardiovasc. Med.* **18**, 228–232
6. Nam, D., Ni, C. W., Rezvan, A., Suo, J., Budzyn, K., Llanos, A., Harrison, D., Giddens, D., and Jo, H. (2009) Partial carotid ligation is a model of acutely induced disturbed flow, leading to rapid endothelial dysfunction and atherosclerosis. *Am. J. Physiol. Heart Circ. Physiol.* **297**, H1535–H1543
7. Bailey, K. A., Haj, F. G., Simon, S. I., and Passerini, A. G. (2017) Atherosusceptible shear stress activates endoplasmic reticulum stress to promote endothelial inflammation. *Sci. Rep.* **7**, 8196
8. DeVerse, J. S., Sandhu, A. S., Mendoza, N., Edwards, C. M., Sun, C., Simon, S. I., and Passerini, A. G. (2013) Shear stress modulates VCAM-1 expression in response to TNF-α and dietary lipids via interferon regulatory factor-1 in cultured endothelium. *Am. J. Physiol. Heart Circ. Physiol.* **305**, H1149–H1157

9. Tsou, J. K., Gower, R. M., Ting, H. J., Schaff, U. Y., Insana, M. F., Passerini, A. G., and Simon, S. I. (2008) Spatial regulation of inflammation by human aortic endothelial cells in a linear gradient of shear stress. *Microcirculation* **15**, 311–323
10. Civelek, M., Manduchi, E., Riley, R. J., Stoeckert, C. J., Jr., and Davies, P. F. (2009) Chronic endoplasmic reticulum stress activates unfolded protein response in arterial endothelium in regions of susceptibility to atherosclerosis. *Circ. Res.* **105**, 453–461
11. Feaver, R. E., Hastings, N. E., Pryor, A., and Blackman, B. R. (2008) GRP78 upregulation by atheroprone shear stress via p38-, alpha2beta1-dependent mechanism in endothelial cells. *Arterioscler. Thromb. Vasc. Biol.* **28**, 1534–1541
12. Zhang, K., Shen, X., Wu, J., Sakaki, K., Saunders, T., Rutkowski, D. T., Back, S. H., and Kaufman, R. J. (2006) Endoplasmic reticulum stress activates cleavage of CREBH to induce a systemic inflammatory response. *Cell* **124**, 587–599
13. Zeng, L., Zampetaki, A., Margariti, A., Pepe, A. E., Alam, S., Martin, D., Xiao, Q., Wang, W., Jin, Z. G., Cockerill, G., Mori, K., Li, Y. S., Hu, Y., Chien, S., and Xu, Q. (2009) Sustained activation of XBP1 splicing leads to endothelial apoptosis and atherosclerosis development in response to disturbed flow. *Proc. Natl. Acad. Sci. USA* **106**, 8326–8331
14. Dagia, N. M., Harii, N., Meli, A. E., Sun, X., Lewis, C. J., Kohn, L. D., and Goetz, D. J. (2004) Phenyl methimazole inhibits TNF-alpha-induced VCAM-1 expression in an IFN regulatory factor-1-dependent manner and reduces monocytic cell adhesion to endothelial cells. *J. Immunol.* **173**, 2041–2049
15. Collins, C., Guilluy, C., Welch, C., O'Brien, E. T., Hahn, K., Superfine, R., Burridge, K., and Tzima, E. (2012) Localized tensional forces on PECAM-1 elicit a global mechanotransduction response via the integrin-RhoA pathway. *Curr. Biol.* **22**, 2087–2094
16. Tzima, E., Irani-Tehrani, M., Kiosses, W. B., Dejana, E., Schultz, D. A., Engelhardt, B., Cao, G., DeLisser, H., and Schwartz, M. A. (2005) A mechanosensory complex that mediates the endothelial cell response to fluid shear stress. *Nature* **437**, 426–431
17. Russell-Puleri, S., Dela Paz, N. G., Adams, D., Chattopadhyay, M., Cancel, L., Ebong, E., Orr, A. W., Frangos, J. A., and Tarbell, J. M. (2017) Fluid shear stress induces upregulation of COX-2 and PGI_2 release in endothelial cells via a pathway involving PECAM-1, PI3K, FAK, and p38. *Am. J. Physiol. Heart Circ. Physiol.* **312**, H485–H500
18. Hoefen, R. J., and Berk, B. C. (2002) The role of MAP kinases in endothelial activation. *Vascul. Pharmacol.* **38**, 271–273
19. Azuma, N., Akasaka, N., Kito, H., Ikeda, M., Gahtan, V., Sasajima, T., and Sumpio, B. E. (2001) Role of p38 MAP kinase in endothelial cell alignment induced by fluid shear stress. *Am. J. Physiol. Heart Circ. Physiol.* **280**, H189–H197
20. Ishida, T., Peterson, T. E., Kovach, N. L., and Berk, B. C. (1996) MAP kinase activation by flow in endothelial cells. Role of beta 1 integrins and tyrosine kinases. *Circ. Res.* **79**, 310–316
21. Jo, H., Sipos, K., Go, Y. M., Law, R., Rong, J., and McDonald, J. M. (1997) Differential effect of shear stress on extracellular signal-regulated kinase and N-terminal Jun kinase in endothelial cells. Gi2- and Gbeta/gamma-dependent signaling pathways. *J. Biol. Chem.* **272**, 1395–1401
22. McCue, S., Dajnowiec, D., Xu, F., Zhang, M., Jackson, M. R., and Langille, B. L. (2006) Shear stress regulates forward and reverse planar cell polarity of vascular endothelium *in vivo* and *in vitro*. *Circ. Res.* **98**, 939–946
23. Surapisitchat, J., Hoefen, R. J., Pi, X., Yoshizumi, M., Yan, C., and Berk, B. C. (2001) Fluid shear stress inhibits TNF-alpha activation of JNK but not ERK1/2 or p38 in human umbilical vein endothelial cells: inhibitory crosstalk among MAPK family members. *Proc. Natl. Acad. Sci. USA* **98**, 6476–6481
24. Yamawaki, H., Lehoux, S., and Berk, B. C. (2003) Chronic physiological shear stress inhibits tumor necrosis factor-induced proinflammatory responses in rabbit aorta perfused ex vivo. *Circulation* **108**, 1619–1625
25. Usami, S., Chen, H. H., Zhao, Y., Chien, S., and Skalak, R. (1993) Design and construction of a linear shear stress flow chamber. *Ann. Biomed. Eng.* **21**, 77–83
26. Foster, G. A., Gower, R. M., Stanhope, K. L., Havel, P. J., Simon, S. I., and Armstrong, E. J. (2013) On-chip phenotypic analysis of inflammatory monocytes in atherogenesis and myocardial infarction. *Proc. Natl. Acad. Sci. USA* **110**, 13944–13949
27. Wang, Y. I., Bettaieb, A., Sun, C., DeVerse, J. S., Radecke, C. E., Mathew, S., Edwards, C. M., Haj, F. G., Passerini, A. G., and Simon, S. I. (2013) Triglyceride-rich lipoprotein modulates endothelial vascular cell adhesion molecule (VCAM)-1 expression via differential regulation of endoplasmic reticulum stress. *PLoS One* **8**, e78322
28. Berk, B. C. (2008) Atheroprotective signaling mechanisms activated by steady laminar flow in endothelial cells. *Circulation* **117**, 1082–1089
29. Zakkar, M., Chaudhury, H., Sandvik, G., Enesa, K., Luong le, A., Cuhlmann, S., Mason, J. C., Krams, R., Clark, A. R., Haskard, D. O., and Evans, P. C. (2008) Increased endothelial mitogen-activated protein kinase phosphatase-1 expression suppresses proinflammatory activation at sites that are resistant to atherosclerosis. *Circ. Res.* **103**, 726–732
30. Zakkar, M., Van der Heiden, K., Luong le, A., Chaudhury, H., Cuhlmann, S., Hamdulay, S. S., Krams, R., Edirisinghe, I., Rahman, I., Carlsen, H., Haskard, D. O., Mason, J. C., and Evans, P. C. (2009) Activation of Nrf2 in endothelial cells protects arteries from exhibiting a proinflammatory state. *Arterioscler. Thromb. Vasc. Biol.* **29**, 1851–1857
31. Lee, J., Sun, C., Zhou, Y., Lee, J., Gokalp, D., Herrema, H., Park, S. W., Davis, R. J., and Ozcan, U. (2011) p38 MAPK-mediated regulation of Xbp1s is crucial for glucose homeostasis. *Nat. Med.* **17**, 1251–1260

Received for publication January 26, 2019.
Accepted for publication August 12, 2019.